AFRL-PR-WP-TP-2006-243

EXPERIMENTAL EVALUATION OF AN INLET PROFILE GENERATOR FOR HIGH PRESSURE TURBINE TESTS

M.D. Barringer, K.A. Thole, and M.D. Polanka

JUNE 2006

STINFO COPY

REPORT DOCUMENTATION PAGE

The public reporting burden for this collection of information is estimated to average 1 hour per response, including the time for reviewing instructions, searching existing data sources, searching existing data sources, gathering and maintaining the data needed, and completing and reviewing the collection of information. Send comments regarding this burden estimate or any other aspect of this collection of information, including suggestions for reducing this burden, to Department of Defense, Washington Headquarters Services, Directorate for Information Operations and Reports (0704-0188), 1215 Jefferson Davis Highway, Suite 1204, Arlington, VA 22202-4302. Respondents should be aware that notwithstanding any other provision of law, no person shall be subject to any penalty for failing to comply with a collection of information if it does not display a currently valid OMB control number. **PLEASE DO NOT RETURN YOUR FORM TO THE ABOVE ADDRESS.**

1. REPORT DATE *(DD-MM-YY)*	2. REPORT TYPE	3. DATES COVERED *(From - To)*
June 2006	Conference Paper Postprint	05/01/2003 – 01/01/2006

4. TITLE AND SUBTITLE

EXPERIMENTAL EVALUATION OF AN INLET PROFILE GENERATOR FOR HIGH PRESSURE TURBINE TESTS

5a. CONTRACT NUMBER
In-house

5b. GRANT NUMBER

5c. PROGRAM ELEMENT NUMBER
N/A

6. AUTHOR(S)

M.D. Barringer and K.A. Thole (Virginia Tech University)
M.D. Polanka (AFRL/PRTT)

5d. PROJECT NUMBER
N/A

5e. TASK NUMBER
N/A

5f. WORK UNIT NUMBER
N/A

7. PERFORMING ORGANIZATION NAME(S) AND ADDRESS(ES)

Turbine Branch (AFRL/PRTT)
Turbine Engine Division
Propulsion Directorate
Air Force Research Laboratory, Air Force Materiel Command
Wright-Patterson Air Force Base, OH 45433-7251

Virginia Tech University
Department of Mechanical
  Engineering
Blacksburg, VA 24060

8. PERFORMING ORGANIZATION REPORT NUMBER

AFRL-PR-WP-TP-2006-243

9. SPONSORING/MONITORING AGENCY NAME(S) AND ADDRESS(ES)

Propulsion Directorate
Air Force Research Laboratory
Air Force Materiel Command
Wright-Patterson AFB, OH 45433-7251

10. SPONSORING/MONITORING AGENCY ACRONYM(S)
AFRL-PR-WP

11. SPONSORING/MONITORING AGENCY REPORT NUMBER(S)
AFRL-PR-WP-TP-2006-243

12. DISTRIBUTION/AVAILABILITY STATEMENT
Approved for public release; distribution is unlimited.

13. SUPPLEMENTARY NOTES

14. ABSTRACT

Improving the performance and durability of gas turbine aircraft engines depends highly on achieving a better understanding of the flow interactions between the combustor and turbine sections. The flow exiting the combustor is very complex, and it is characterized primarily by elevated turbulence and large variations in temperature and pressure. To better understand these effects, the goal of this work is to benchmark an adjustable turbine inlet profile generator for the Turbine Research Facility (TRF) at the Air Force Research Laboratory (AFRL). The research objective was to experimentally evaluate the performance of the non-reacting simulator that was designed to provide representative combustor exit profiles to the inlet of the TRF turbine test section. This paper discusses the verification testing that was completed to benchmark the performance of the generator. Results are presented in the form of temperature and pressure profiles as well as turbulence intensity and length scale. This study shows how one combustor geometry can produce significantly different flow and thermal field conditions entering the turbine.

15. SUBJECT TERMS
Pressure Profiles, Temperature Profiles, Turbulence Profiles Combustor Interaction on Turbine Vane

16. SECURITY CLASSIFICATION OF:			17. LIMITATION OF ABSTRACT:	18. NUMBER OF PAGES	19a. NAME OF RESPONSIBLE PERSON (Monitor)
a. REPORT Unclassified	**b. ABSTRACT** Unclassified	**c. THIS PAGE** Unclassified	SAR	18	Marc Polanka
					19b. TELEPHONE NUMBER *(Include Area Code)* N/A

Experimental Evaluation of an Inlet Profile Generator For High Pressure Turbine Tests

M. D. Barringer and K. A. Thole
Mechanical Engineering Department
Virginia Polytechnic Institute and State University
Blacksburg, VA 24061

M. D. Polanka
Air Force Research Laboratory
Turbines Branch
WPAFB, OH 45433

ABSTRACT

Improving the performance and durability of gas turbine aircraft engines depends highly on achieving a better understanding of the flow interactions between the combustor and turbine sections. The flow exiting the combustor is very complex and it is characterized primarily by elevated turbulence and large variations in temperature and pressure. The heat transfer and aerodynamic losses that occur in the turbine passages are driven primarily by these spatial variations. To better understand these effects, the goal of this work is to benchmark an adjustable turbine inlet profile generator for the Turbine Research Facility (TRF) at the Air Force Research Laboratory (AFRL).   The research objective was to experimentally evaluate the performance of the non-reacting simulator that was designed to provide representative combustor exit profiles to the inlet of the TRF turbine test section. This paper discusses the verification testing that was completed to benchmark the performance of the generator. Results are presented in the form of temperature and pressure profiles as well as turbulence intensity and length scale. This study shows how one combustor geometry can produce significantly different flow and thermal field conditions entering the turbine. Engine designers should place emphasis on obtaining accurate knowledge of the flow distribution within the combustion chamber as this can result in significantly different inlet profiles to the turbine that can change local aerodynamics and heat transfer within the turbine.

NOMENCLATURE

C   vane axial chord length

Cp   pressure coefficient, $Cp = \dfrac{P_0 - P_{0_{ms}}}{\frac{1}{2}\rho_{AVE}U^2_{AVE}}$

D   dilution hole diameter

I   momentum flux ratio, $I = \dfrac{\rho_{jet}U^2_{jet}}{\rho_\infty U^2_\infty}$

M   Mach number
P   pressure or vane pitch
R   autocorrelation coefficient

Re   Reynolds number, $Re = \dfrac{U_{AVE}\cdot C}{\nu}$

S   vane span
T   temperature
Tu   turbulence intensity, $Tu = U_{RMS}/U_{AVE}$
U   velocity
X,Y,Z   axial, pitch, and span directions

Greek

T integral time scale, $T = \int_0^\infty R(\tau)d\tau$

Λ integral length scale, $\Lambda = T\cdot U_{AVE}$
ν kinematic viscosity
ρ density
τ autocorrelation time lag
θ temperature coefficient, $\theta = (T - T_{AVE})/T_{AVE}$

Subscripts

∞ freestream or mainstream
1, 2   dilution row number
AVE   average
FC   film cooling
jet   flow exiting hole
max   maximum
MS   mid-span
RMS   root-mean-square

INTRODUCTION

Increasing the thrust to weight ratio of a gas turbine aircraft engine can be accomplished by increasing the turbine working temperature. This has put great emphasis on understanding just how the combustor exit flow interacts with and affects the performance of the downstream turbine.   The complex temperature and pressure profiles exiting combustors have forced engine designers to prepare for the worst case without knowing exactly how the profiles affect the hardware.   The variations in pressure, temperature, and turbulence that are present in the radial and circumferential spatial directions at the combustor exit all combine to yield a very complex exit flow structure.   Modern combustors are migrating towards less

POSTPRINT

circumferential temperature variation however radial profiles will continue to dominate the combustor exit profile. These temperature variations migrate through the combustion chamber and impose non-uniform heat transfer on the downstream high pressure turbine vanes that can result in local melting and cracking of the vane metal and in some circumstances result in total failure of the part. Elevated turbulence can intensify this heat transfer by increasing local convection heat transfer coefficients to the vane surface making it essential to properly replicate this effect in the turbine. Turbine designers currently use a pressure profile consistent with a standard turbulent boundary layer as the inlet condition to the turbine while designing their vanes and blades. The non-uniformity of the combustor exit pressure profiles can result in turbine inlet profiles that are different than what is expected when using uniform profiles. Spatial variations in pressure at the combustor exit result in non-uniform aerodynamic loading on the vanes and variability in the secondary flow development.

Combustion chambers in aircraft gas turbine engines consist of annular liners, inlet swirlers, fuel nozzles, dilution holes, film cooling holes and slots, and an overall exit contraction. The design of combustion chambers centers on the division of mass flow into separate flow paths to establish continuous stable combustion, to dilute the combustion products before they enter the turbine stage, and to form a protective layer of insulating air that shields the liner metal from the relatively hot combustion gas. The interaction of the flow streams passing through these combustor components results in a complex flowfield exiting the combustor.

A better understanding of how the combustor exit flow affects the flow development and heat transfer within the downstream turbine is needed. It is for this reason that a device was designed to simulate the conditions exiting typical engine combustors by replicating the features of real combustors. The primary research objective was to perform benchmark tests on a non-reacting combustor simulator device. The simulator, documented in Barringer et al. [1], was designed to provide representative combustor exit pressure and temperature profiles, with realistic turbulence levels, to the inlet of the true scale, fully annular, high pressure turbine rig located in the TRF at AFRL. The focus of this paper is to present the benchmark test results. The effects of these different profiles on turbine vane heat transfer and aerodynamics are presented in a separate research paper, Barringer et al. [2].

RESEARCH FOCUS AND PAST STUDIES

Several non-reacting and reacting studies have been performed experimentally and computationally to analyze and model combustor flows. Very few of these studies, however, have focused on the effects that the exit flowfield has on the downstream turbine stage. The following is a review of several past combustor studies as well as several combustor-turbine interaction studies. The combustor studies pertain to analyzing and correctly modeling the flow and thermal fields within the combustion chamber itself whereas the combustor-turbine interaction studies focus on researching the effects of the combustor exit flow on the downstream turbine.

COMBUSTORS

Dilution holes were studied by Holdeman [3] using a non-reacting combustor model. Experiments and computations were conducted on the mixing of single, double, and opposed rows of dilution jets. The principle finding was that the jet momentum flux ratio dictated the combustor exit velocity and temperature profiles. The opposed rows of jets resulted in the most effective and rapid mixing. Computational models using the standard k-ε turbulence model did not accurately predict the mixing of opposed dilution jet injection, but predicted the jet penetration very well.

High-intensity, large-scale turbulence in a non-reacting combustor simulator was studied by Ames and Moffat [4]. Their experimental model contained two rows of in-line dilution holes, and a 50% exit contraction that generated turbulence intensity levels up to 19% and integral length scales that scaled well with the dilution hole diameters. Barringer et al. [5] and Stitzel and Thole [6] also tested and computationally modeled a non-reacting combustor simulator containing liners with film cooling holes and two rows of in-line dilution jets that produced similar turbulence intensity levels near 18%. The computational models used the RNG k-ε turbulence model and the results agreed with those found by Holdeman [3] in that turbulence was underpredicted.

Swirl driven inlet flow was studied by Cameron et al. [7] in non-reacting and reacting model combustors with wall injection. They concluded that the strong recirculation zone located upstream of the primary jets present in the non-reacting case was dissipated in the case of reaction. Velocity measurements in the exit plane indicated turbulence levels near 25% for the reaction case, which is consistent with the studies without reaction.

Turbulence was also studied in two reacting models by Bicen et al. [8] that included liner cooling slots and two rows of dilution jets. The results indicated non-uniform distributions of velocity in the combustor exit plane and turbulence levels near 20% over the majority of the exit plane. These levels are consistent with the results presented earlier for the non-reacting combustor studies indicating that reactions do not significantly contribute to turbulence levels. The temperature profiles at the combustor exit plane were also found to be non-uniform.

COMBUSTOR-TURBINE INTERACTIONS

A combustor exit radial temperature simulator (CERTS) was used by Schwab et al. [9] at the NASA Lewis Research Center to conduct analytical and experimental studies of flow through a full turbine stage with uniform and non-uniform inlet radial temperature profiles. The profiles were generated by adjusting the coolant air mass flow rate injected through circumferential slots in the hub and tip endwalls upstream of the stator vanes. In addition to measuring non-uniform temperature profiles, non-uniform total pressure profiles were indicated at the turbine vane inlet. Cattafesta [10] conducted similar experiments to study the effects of turbine inlet radial temperature profiles on the aerodynamic performance of a transonic turbine stage using the M.I.T. Blow Down Turbine facility. Tests with similar corrected flow conditions but with different temperature profiles affected the overall turbine efficiency by 2%. Results also showed that the turbine inlet profiles were nearly mixed out at the exit plane of the rotor. Chana et al. [11] also designed and tested a non-uniform inlet

temperature generator for the QinetiQ transient turbine research facility. Cold gas was injected upstream of the turbine section at the hub and tip to shape the temperature profile in the radial direction and through turbulence rods inserted into the main flow to shape it in the circumferential direction. Results showed vane heat transfer was affected by the presence of the non-uniform temperature profiles on the vane suction surface.

Krishnamoorthy et al. [12] investigated the effect of combustor turbulence on a downstream turbine vane cascade. Their results indicated that the effect of high turbulence at the combustor exit was to reduce the cooling effectiveness on the vane by 10%. It was also shown that the effect of temperature non-uniformities at the combustor exit was to reduce the overall cooling effectiveness on the vane by as much as 21%. Van Fossen and Bunker [13] studied heat transfer augmentation in the stagnation region of a flat plate with an elliptical leading edge. The test article was located downstream of an arc segment of a dual-annular combustor. The swirl driven combustor flow produced turbulence intensities up to approximately 32% with length scales near 1.3 cm. Augmentation of heat transfer was found to be very significant in the range of 34 to 59%. No effect of circumferential position with respect to the upstream swirlers was found.

Colban et al. [14] studied the effects of varying film cooling flow through the liner and exit junction slot in a large-scale (9X), low speed combustor simulator on the adiabatic effectiveness and secondary flow development within a downstream turbine cascade. Results showed that varying the coolant injection through the liner led to different total pressure profiles entering the downstream turbine section. Measurements showed that the coolant exiting the liner and slot accumulated along the suction side of the vane and endwall and that increasing the film cooling flow through the liner did not result in a continual increase in adiabatic effectiveness values.

In summary, the literature indicates that the most significant components that contribute to the non-uniform exit thermal and pressure fields are swirlers, film cooling slots and holes, and dilution holes. The studies also indicate that thermal fields downstream of the primary dilution zone are very similar with or without reaction. The only noteworthy differences occur upstream of the primary zone where combustion is stabilized. This is important because it allows a flow field representative of one exiting a real gas turbine combustor to be simulated under non-reacting conditions without swirl. There is insufficient research to date; however, that incorporates the effects of realistic combustor flow and thermal fields on downstream turbine vanes and endwall regions. Very little experimental data exists that documents total pressure profiles at the combustor exit. This information is paramount since it has been shown in Hermanson and Thole [15] and Colban et al. [14] that the total pressure field is a driving force in the development of secondary flows and heat transfer present in the downstream turbine vane passages.

EXPERIMENTAL FACILITY

The TRF is a turbine test facility located within the Turbine Engine Research Center at the AFRL at Wright-Patterson Air Force Base in Dayton, Ohio. The TRF, documented in Haldeman et al. [16], is a short duration blow-down test facility that is capable of matching several aero-thermal engine parameters. These parameters include Reynolds number, Mach number, pressure ratio, gas to metal temperature ratio, corrected speed, and corrected mass flow.

The facility, shown in Figure 1, consists primarily of a large supply tank, a turbine test section, and two large vacuum tanks. The test section is a true scale, fully annular, single turbine stage consisting of vanes and rotor blades. Prior to testing, nitrogen gas is pressurized and heated within the supply tank while the main turbine section and vacuum tanks are evacuated to near vacuum conditions. The turbine rotor is then driven by a starting motor to a speed slightly higher than the desired test speed. This motor is then turned off allowing the turbine rotor to decelerate to the test speed at which time an electrical eddy current brake is used to hold the rotor speed constant. Testing begins by activating a fast acting valve that connects the supply tank to the turbine test section. The gas then flows from the supply tank through the turbine test section and into the vacuum tanks. The mass flow rate is set by controlling the turbine pressure ratio using a variable area isolation valve located downstream of the main test section. The duration of a typical test is between one and five seconds, depending on the size of the turbine that is being tested. All testing in the current study was performed in a vane-only configuration (without rotating turbine blades).
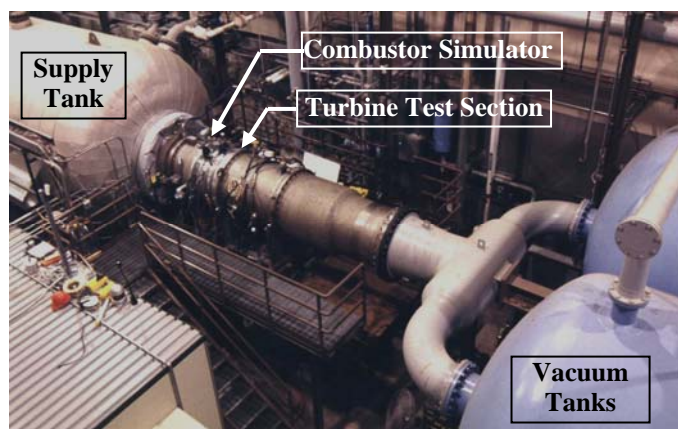

Figure 1. Photo of the TRF facility.

Recently a combustor simulator was designed and installed into the TRF facility to allow turbine testing to be performed with realistic turbine inlet profiles of pressure and temperature. Prior to installing the simulator, the temperature and pressure profiles at the inlet of the turbine section were nearly uniform in the radial and circumferential directions. The simulator, shown in Figure 2 and documented in Barringer et al. [1], divides the supply tank flow into three concentric annular flow paths. The center annulus is further divided into three concentric annuli to direct a portion of the supply tank flow to the inlet of the central annular chamber, shown in Figure 3, and to the first of two rows of dilution holes. The inner and outer annular flow paths are used to thermally condition portions of the supply tank flow by directing the flow through finned-tube heat exchangers and then into the central chamber through secondary dilution holes and film cooling holes located within the contraction section. The first row of opposing dilution jets acts as the primary turbulence generator by injecting flow at relatively large local momentum flux ratios. The second row dilution jets and film cooling jets were designed to inject flow at lower momentum flux ratios to tailor the exit temperature profile.

Direct flow control is accomplished through the use of five adjustable shutter systems. Each system consists of one rotating disc and one non-rotating disc that both contain the exact same slot pattern. By positioning the rotating disc with respect to the non-rotating disc the blockage in a particular flow stream can be increased or decreased. This flow blockage acts as an adjustable pressure drop that allows the flow in a particular path to be controlled. The center shutter system is located at the inlet of the central chamber and it is used to establish the primary flow blockage required to achieve the various flow splits and momentum flux ratios.
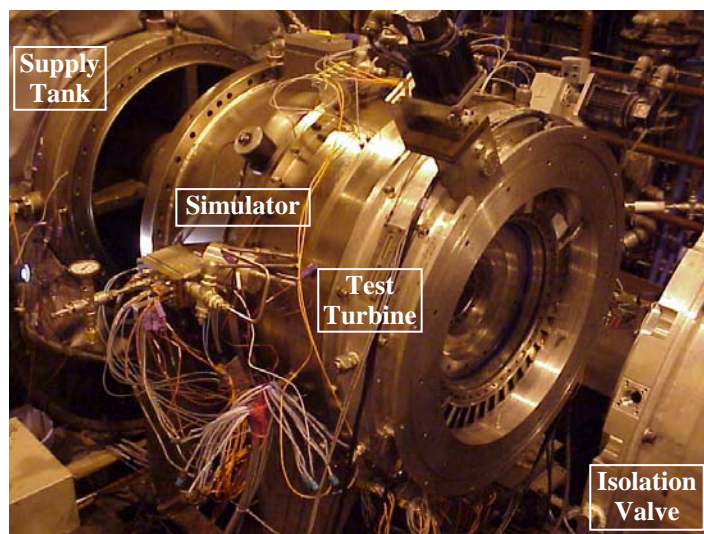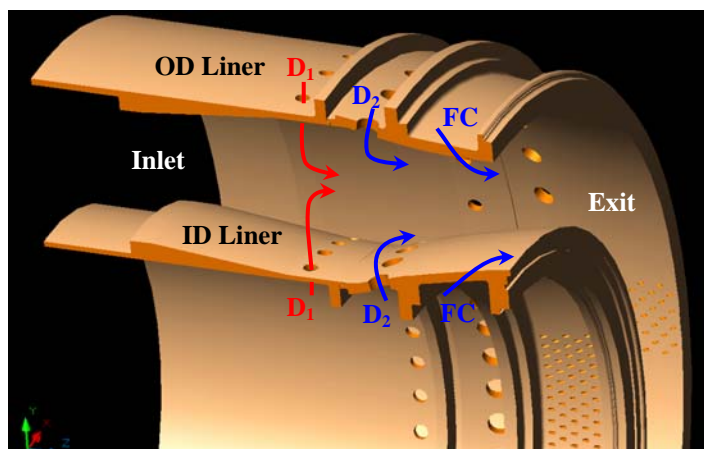

Figure 2. Photo of the TRF combustor simulator.

Figure 3. Drawing of the central annular chamber.

INSTRUMENTATION

Traverse rings are used to measure the turbine inlet and exit conditions. Each traverse ring contains multiple instrumentation rakes for mounting thermocouples and pressure transducers. The probes on each rake are spaced to obtain measurements over equal annular flow areas and during testing these rakes are traversed circumferentially by approximately 90 degrees to obtain both radial and circumferential profiles. Due to the short test duration, measurements of temperature and pressure as well as velocity, heat flux, and rotor speed are all recorded simultaneously in real time onto data storage units. The facility is capable of simultaneously acquiring data across 200 12-bit channels with a maximum sampling frequency of

100 kHz and 200 16-bit channels with a maximum sampling frequency of 200 kHz. Signal conditioning on each channel takes place using low pass filters and built-in amplifiers. All data processing and reduction is performed at a later time.

For the current tests, three temperature rakes were used each containing 0.0254 mm diameter thermocouple beads with a thermal time constant of approximately 1.1 milliseconds. The three rakes included one containing five beads, one with seven beads, and one with nine beads. The different number of beads provides more spatial radial locations to perform ensemble averaging. Two pressure rakes were used each containing nine pressure transducers. All flow and thermal field measurements taken during testing were sampled at 20 kHz. To benchmark the performance of the simulator, measurements of total pressure, static pressure, velocity, flow temperature, and surface temperature were taken. An instrumentation plan was developed to locate the places within the simulator to perform these measurements. Figure 4 shows a drawing of the simulator highlighting these positions and their measurements.

Total pressure measurements were made using in-house custom Kiel probes that were positioned within the plenums of the second row dilution holes and film cooling holes to help quantify mass flow splits between the various flow paths. Kiel probes were also positioned at the exit of several dilution holes to help verify the amount flow passing through both dilution rows. Static pressure measurements were made on the surface of the inner and outer diameter contraction liners at an axial location upstream of the film cooling holes to help determine the amount of flow exiting the film cooling holes. These static pressure measurements were made using high-temperature, miniature, Kulite pressure transducers. Velocity measurements were also made using several custom pitot-static pressure probes placed upstream and downstream of each heat exchanger and the central chamber shutter system.
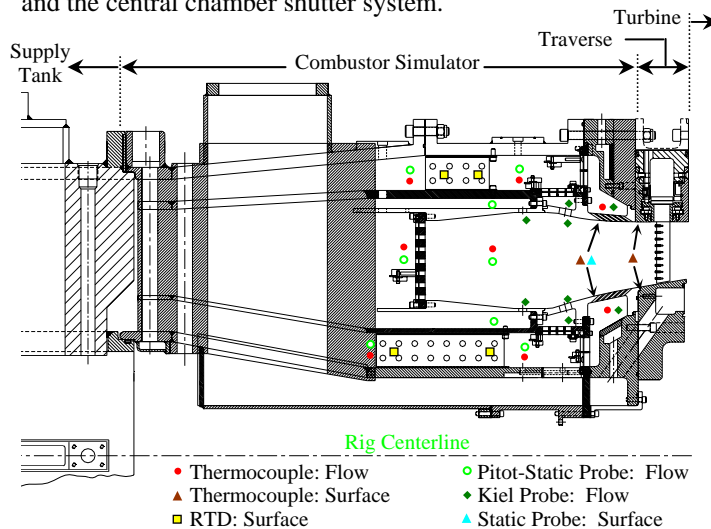

Figure 4. General instrumentation locations.

The pressure transducers were calibrated in situ prior to each run. A Ruska standard was used to monitor the test section pressure while it was filled and evacuated. A typical calibration uncertainty for the static transducers was less than 0.05% of full scale. The overall uncertainty for these transducers was raised 0.40% due to short term drift known to exist between time of calibration and time of the run. The velocity measurements were more uncertain. This was

4

attributed to the very small delta pressures (less than 6000 Pascals) that were measured at these locations coupled with the fact that these transducers were not able to be calibrated each run resulting in a long term drift uncertainty as well. This was further compounded by the fact that these are single point measurements both across the annuli and around the circumference making it difficult to know what the true average annulus velocity was. Converted to massflow, uncertainties up to 10% were possible.

The flow temperature at various locations within the simulator was measured using in-house type E thermocouple probes containing 0.127 mm diameter beads. These thermocouple probes were used to monitor the flow temperature within the film cooling plenums as well as upstream and downstream of the heat exchangers. The heat exchanger metal temperatures were monitored before and during testing using Omega RTD's. The metal temperatures of the inner and outer diameter contraction rings were monitored using type E thermocouples with 0.076 mm diameter beads. The thermocouple wire that made these beads was calibrated in a Kaye temperature bath against a platinum RTD standard accurate to 0.01 K. The 0.127 mm beads were calibrated and found to be within 1.0 K of the standard E type curve. The 0.0254 mm beads in the rakes were calibrated to an accuracy of 1.5 K but had a noticeable shift from the standard E type thermocouple curve due to the imperfections of the wire.

In addition to measuring the pressure and temperature profiles exiting the simulator, the traverse ring located upstream of the turbine test section was modified to incorporate a special hotwire rake to allow measurements of velocity at the simulator exit. The rake allowed for the mounting of two hot-film probes with their sensing elements positioned near vane mid-span at $Z/S = 0.45$ and 0.55. The hotwire probes were calibrated outside of the main test rig at ambient temperature and pressure using a TSI flow calibration unit. The calibration curves for the probes both follow a power law curve fit for wire Nusselt number versus Reynolds number. Since the velocity at the simulator exit is near $M = 0.1$ during testing, a simple density correction was applied to the experimental test data in order to apply the curve fits to the higher density flow exiting the simulator. Due to the transient nature of the test rig and the varying elevated flow temperatures, hotwire measurements were conducted under separate isothermal test conditions (unheated supply tank) where all flow streams were approximately at the same temperature near ambient conditions.

TEST MATRIX

A series of benchmark tests was developed to determine the overall performance of the simulator device. These tests were determined by performing a Taguchi style analysis, described in Roy [17], to help reduce the number of experimental runs needed to produce a performance map for the combustor simulator. Nine factors were selected as the system inputs including the initial supply tank temperature and pressure, the initial metal temperatures of the two heat exchangers, and the porosities of the five adjustable shutters. Porosity refers to the percentage of total open flow area of the shutter. Each of the input factors was assigned an upper and lower limit, shown in Table 1, which was based on component operating limits.

TABLE 2. Experimental Test Matrix (Baseline and *Additional Re* Tests)

| Test | Supply Tank | | Percent of Total Mass Flow (%) | | | | | | | Heat Exchanger: Initial T(K) | |
	T (K)	P (kPa)	Central Chamber Inlet	ID 1st Row Dilution	OD 1st Row Dilution	ID 2nd Row Dilution	OD 2nd Row Dilution	ID Film Cooling	OD Film Cooling	Inner Annulus	Outer Annulus
104	480	200	54	8	7	5	14	0	12	300	300
105	480	200	6	13	12	20	24	1	24	300	400
106	480	200	12	13	12	7	27	9	20	400	300
107	480	550	14	12	11	14	22	8	19	300	300
108	480	550	52	7	7	4	14	4	12	300	400
109	480	550	48	7	7	9	15	0	14	400	300
110	340	200	50	7	8	7	15	2	11	300	300
111	340	200	15	12	12	8	22	9	22	300	400
112	340	200	52	8	8	5	14	1	12	400	400
113	340	200	9	14	13	16	23	3	22	400	300
114	340	550	53	8	7	9	10	1	12	300	400
115	480	550	15	14	13	9	24	0	25	400	400
116	480	200	54	9	8	9	11	5	4	400	400
117	340	550	15	15	15	12	32	3	8	300	300
118	340	550	57	9	8	5	12	5	4	400	300
119	340	550	8	13	12	13	25	8	21	400	400
120	340	200	15	17	16	13	22	13	4	300	400
121	340	200	53	9	9	8	15	2	4	400	400
122	480	550	14	15	14	18	27	8	4	300	300
123	480	550	56	8	8	9	18	0	1	400	300
124	480	550	40	11	11	4	20	4	10	300	300
125	480	550	37	11	11	6	21	4	10	400	400
126	420	550	64	7	8	7	14	0	0	400	400
127	420	550	61	6	6	2	9	4	12	400	400
133	420	550	36	13	13	14	15	9	0	300	400
134	420	550	32	11	10	5	22	0	20	400	300
135	480	550	23	13	12	5	13	10	24	300	300

TABLE 1. High and Low Values of System Inputs

System Inputs	Unit	Low	High
Initial Pressure: Supply Tank	kPa	207	552
Initial Temp: Supply Tank	K	366	478
Initial Temp: ID Heat Exchangers	K	297	422
Initial Temp: OD Heat Exchangers	K	259	422
Porosity: Central Chamber Shutter	%	30	90
Porosity: ID Film Cooling Shutter	%	12	89
Porosity: OD Film Cooling Shutter	%	10	90
Porosity: ID 2nd Row Dilution Shutter	%	13	93
Porosity: OD 2nd Row Dilution Shutter	%	14	98

The system outputs are the pressure and temperature profiles at the combustor simulator exit, and therefore consist of a set of pressure probes and a set of thermocouple probes that are mounted on separate instrumentation rakes. These probes were traversed approximately ninety degrees in the circumferential direction during testing to determine both radial and circumferential variations in pressure and the temperature. The benchmark tests that were determined from the analysis are shown in Table 2 and they provided a large data set that includes over two dozen different combinations of combustor exit temperature and pressure profiles. The test cases shown in Table 2 that are in bold correspond to the baseline experiments where the mean flow conditions at the simulator exit (turbine vane inlet) are $Re = 2.1 \times 10^5$ and $M = 0.1$. Additional tests were performed at different Reynolds numbers to create a more complete performance map of the simulator, including $Re = 0.8 \times 10^5$, 1.1×10^5, and 2.7×10^5. These additional Re tests are shown in Table 2 in italics. All experimental data associated with a particular test configuration was acquired during a single blow-down test.

The knowledge gained from these tests comes in the form of a sensitivity coefficient for each input factor and how it affects the exit profiles at certain radial locations. Determining the sensitivities of all nine inputs was accomplished by performing a statistical analysis of variance. This analysis mapped each system input setting to the measured system outputs and also estimated the sensitivity of interactions between individual system inputs. The procedure for performing this analysis is also outlined in Roy [17].

RADIAL PRESSURE PROFILE RANGE

The radial pressure profiles measured at the simulator exit for the baseline test cases are shown in Figure 5 (test numbers are shown in Table 2). These radial profiles have been circumferentially (spatially) averaged across one full vane pitch along lines of constant radius that correspond to equal annular flow areas. Data was analyzed across several vane pitches that are all equally spaced around the entire 360 degrees annulus. The local total pressure has been normalized into the form of a pressure coefficient C_p, defined as the local total pressure subtracted by the mid-span total pressure all divided by the mean dynamic pressure at the simulator exit. Radial pressure profiles are often referenced with respect to a span location, for example inner diameter (ID) peaked, outer diameter (OD) peaked, or mid-span peaked. The normalization used here is consistent with this idea in that it compares each local total pressure to that at the midspan. Note that in using this definition, $C_p = 0$ at the midspan.
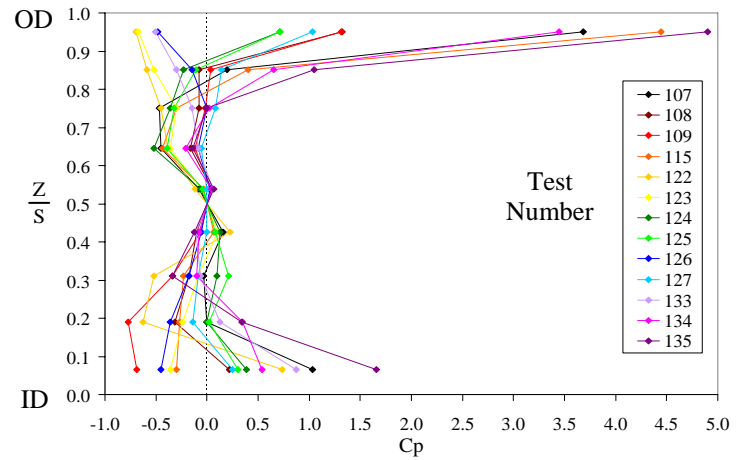
Figure 5. Plot of several radial pressure profiles measured at the simulator exit for the baseline tests.
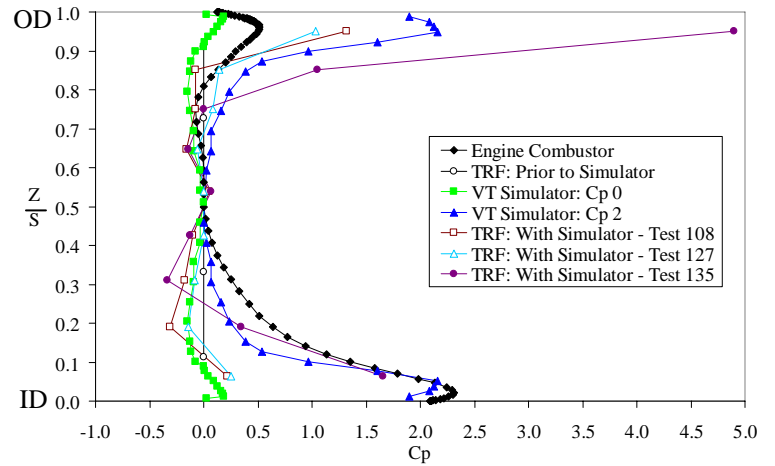
Figure 6. Plot of several engine and combustor simulator exit pressure profiles.

The measured C_p values near the endwalls on both the ID and OD are consistent with those exiting real combustors. Figure 6 shows an example of a pressure profile at the exit of an aero-engine combustor, as well as three pressure profiles generated using the TRF simulator and two generated using the Virginia Tech simulator. The TRF simulator was designed using this engine profile and the Virginia Tech (VT) simulator profiles, documented in Barringer et al. [5] and Colban et al. [14]. Figure 6 also shows the pressure profile at the TRF turbine inlet prior to installing the simulator. It can be seen from the figure that the TRF simulator can produce turbine inlet pressure profiles similar to those of the VT simulator and the engine profile. The test conditions shown here were not configured to specifically match any of these engine cases, but show that these different profiles can be achieved within the simulator's range. For example, the profiles corresponding to tests 108 and 127 result in pressure profiles similar to the *VT Simulator C_p 0.0* curve on the ID side and the *VT Simulator C_p 2.0* curve on the OD side. The TRF simulator can easily shift the profile peak near the endwalls from $C_p = 0$ to 2 to be consistent with the engine profile. It is important to note that the VT and TRF combustor simulators are completely different experimental rigs. The VT simulator is a large scale linear device that operates at relatively low pressure, low speed, and low

temperature, while the TRF simulator is a true-scale fully annular device that operates at high pressure, high speed, and elevated temperatures.

The pressure profiles that are plotted in Figure 5 vary greatly in overall shape, especially near the ID and OD endwalls. Some of the profiles are peaked along the ID and OD endwalls and some are peaked in the mid-span region. At the baseline flow conditions, the simulator is capable of producing pressure profiles in the near ID endwall region between $-0.7 < C_P < 1.7$ and in the near OD endwall region between $-0.6 < C_P < 5.0$. It is important to note that a negative C_P does not mean that flow is in the opposite direction or that the pressure is negative, it simply means that the local pressure is less than the mid-span pressure. For example, the pressure profile corresponding to test 126 is mid-span peaked. The pressure profile operating range is larger on the OD side than the ID side. This was expected due to the outer annulus possessing less overall flow resistance compared to the inner annulus and the fact that the central chamber contraction is larger on the ID side than the OD side, which was an original design constraint to accommodate the radial dimensions of the turbine being tested. But nonetheless, the simulator is capable of achieving C_P values consistent with the range of the real engines, i.e. up to 2.0.

To create a more complete performance map of the simulator, several tests were also conducted where the flow conditions at the simulator exit were at different Reynolds numbers. These tests, corresponding to Re = 0.8 x 10^5, 1.1 x 10^5, 2.7 x 10^5, are given in Table 2 in italics. The measured radial pressure profiles for some of these tests are shown in Figure 7. These radial profiles have also been circumferentially averaged over one vane pitch. The results shown in this figure highlight that the inlet profile generator is capable of producing realistic turbine inlet profiles over a wide range of operating points. This is important for future tests as it shows the flexibility of the simulator to generate any desired inlet condition throughout a turbine operating map. Pressure profiles measured in the near ID endwall region ranged from $-0.6 < C_P < 2.0$ while near the OD endwall region they ranged from $-0.6 < C_P < 5.0$.
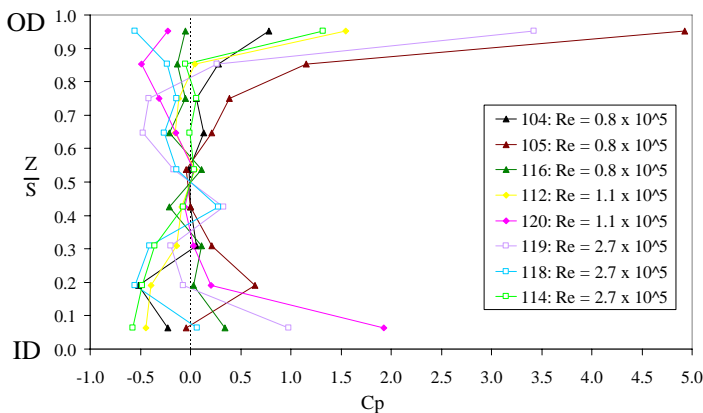
endwalls results in a negative C_P value. As the film cooling mass flow is increased the momentum flux ratio of the film cooling jets increases which forces more flow out into the mainstream along the endwalls. This results in a higher total pressure near the endwall relative to mid-span. As the film cooling flow is increased even further, the local total pressure near the endwall becomes significantly higher than that in the mid-span region resulting in the sharp gradients seen in some of the profiles. The spanwise variation in the pressure coefficient was found to be less in the span region from $0.25 < Z / S < 0.75$. This smaller variation is explained by the intense mixing process of the upstream dilution jets that inject large amounts of flow into the central chamber producing high turbulence levels. As this flow progresses down the axis of the central chamber the individual dilution jets expand and merge into one another. This turbulent process results in a large mixing zone over the majority of the chamber span thereby reducing spatial variations. This effect was also confirmed by the CFD computation of Kunze et al. [18] for these same test runs.

The measured peak in the C_P pressure profile near the endwalls is scaled in Figure 8 to the film cooling momentum flux ratio as well as the combustor simulator exit Reynolds number. The figure shows that as the momentum flux ratio is increased, the measured peak in the C_P pressure profile increases in a parabolic but nearly linear manner. The curves that are shown are parabolic best fits of the data points. The figure shows that the ID film cooling possesses a slightly less powerful trend than the OD for a given momentum flux ratio. This is explained by the fact that as the film cooling on the ID side exits the holes it must pass over a large contracting surface, relative to the OD side. This ID contraction forces the film cooling flow to move outward in the radial direction and by the time it reaches the axial location of the instrumentation rake its momentum has been reduced relative to the film cooling flow along the OD side. As the film cooling on the OD side exits the holes, it sees a relatively constant annular flow area and a relatively short direct path to the instrumentation rake. Figure 8 also shows that as the Reynolds number at the combustor simulator exit increases the measured peak in the C_P pressure profile along the endwall has a slightly decreasing trend for a given film cooling momentum flux ratio. Overall, the results were similar for both the ID and OD endwall regions.

Figure 7. Several pressure profiles measured at the simulator exit at different Reynolds numbers.

The wide range of C_P values in the near endwall regions is directly attributable to the relative amount of upstream film-cooling flow. When the film cooling mass flow is significantly low the local total pressure at span locations near the
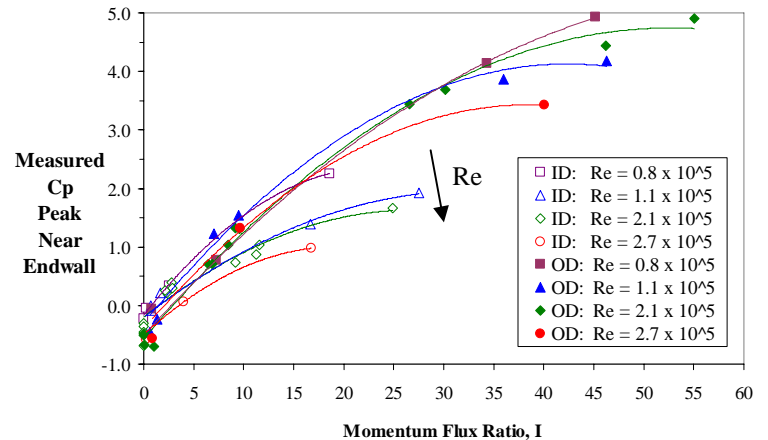

Figure 8. Plot of the pressure profile peak (measured) near the ID and OD endwalls scaled to the film cooling momentum flux ratio and simulator exit Re number.

An attempt was also made to scale the pressure profiles at the exit of the simulator to the dilution flow conditions which primarily affects the mid-portion of the flow path. Figure 9 shows

7

two distinct patterns that were observed between $0.4 < Z/S < 0.8$ that scaled to the total amount of dilution mass flow. The first group consists of tests in which the total dilution mass flow was in the range of 23-38% of the total combustor flow, and the second group was tests in which the total dilution mass flow was in the range of 43-74% of the total combustor flow. The first group is relatively uniform in this span, while the second group contains a significant backwards facing gradient in the span direction. It can be seen that this gradient exists for tests cases with little to no film cooling on the OD side as well as test cases with large amounts of film cooling on the OD side, as indicated by the C_p values near the OD. This is important because it indicates that the gradient truly is a direct result of the dilution flow. This effect was further confirmed by investigation of the CFD results of Kunze [18] which highlighted that the second row of OD dilution jets has a strong influence in shaping the flow profile in this region.
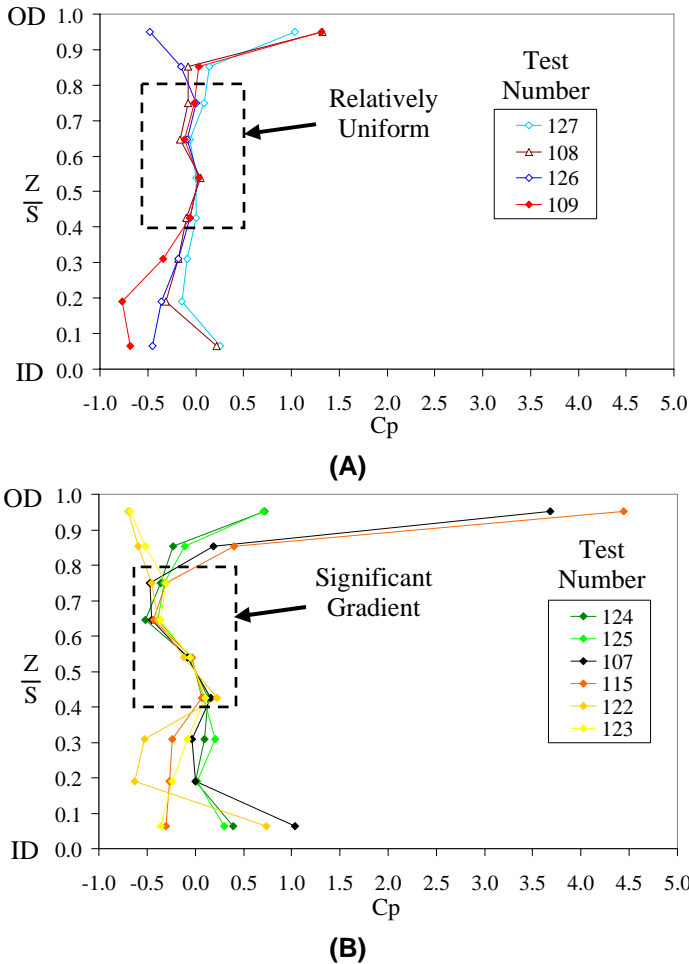

(A)

(B)

Figure 9. Plots of pressure profiles at the simulator exit when the total dilution mass flow is (A) 23-38% and (B) 43-74% of the total combustor exit flow.

RADIAL TEMPERATURE PROFILE RANGE

The combustor exit temperature profile can be arranged in several non-dimensional forms. Engine manufacturers typically use the pattern factor P.F. = $(T_{max} - T_{ave}) / \Delta T_{combustor}$ to document the performance of their combustors. This pattern factor definition, however, only applies to actual combustors as it references the temperature rise across the

combustor. In a simulator, the inlet condition is irrelevant and only the profiles entering the turbine are of interest. The radial temperature profiles measured at the simulator exit for the baseline tests are shown in Figure 10 for the seven-headed thermocouple rake. These radial profiles have also been circumferentially averaged across one full vane pitch. The local total temperature has been normalized into the form of the temperature coefficient θ, defined as the local total temperature subtracted by the average temperature at the simulator exit all divided by the same average temperature.

The average temperature at the simulator exit was determined by performing an integration from hub to tip of the spanwise profile. To obtain a better approximation of this average temperature, the temperature profile data was extrapolated to the endwalls using a constant slope between the outer most and second outer most data points. The figure shows a variety of temperature profiles including some that are mid-span peaked (107), some that are peaked more towards the ID (109), some that are peaked more towards the OD (108), and some that are nearly uniform in the mid-span region (125 and 127). The temperature profiles near the ID and OD endwalls show large differences, some are nearly uniform (133 and 134) and some possess sharp gradients (108, 109, and 135). The test case numbers refer to the test conditions given in Table 2.
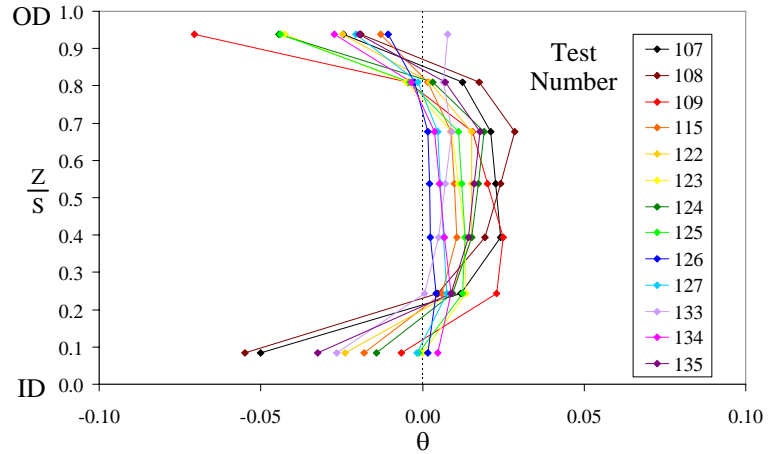

Figure 10. Plot of several radial temperature profiles measured at the simulator exit for the baseline tests.
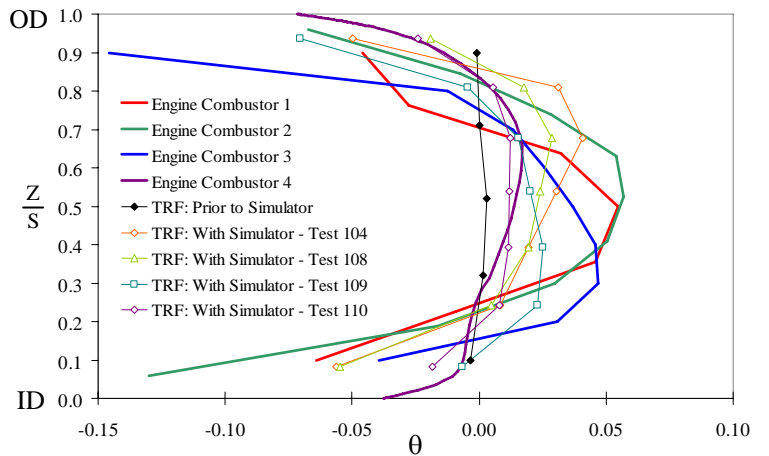

Figure 11. Plot of several engine and simulator combustor exit temperature profiles.

The measured θ profiles are similar to those exiting real combustors. Figure 11 shows several temperature profiles at the exit of aero-engine combustors, as well as temperature profiles at the TRF turbine inlet prior to and after installing the simulator. These aero-engine profiles were used to help design the TRF simulator. The figure shows that the TRF simulator is capable of producing turbine inlet temperature profiles similar to those of the engine profiles. While these profiles are not identical to the engine cases, (and again efforts were not made in this program to tailor the profile to a particular case) they do enable researchers and designers the ability to understand the effects that these profiles have on vane and rotor heat transfer bettter than conventional uniform inlet profiles.

The maximum radial temperature variation that was observed using the seven - headed thermocouple rake for the baseline tests was approximately Δθ = 0.10 or 10%, which corresponds to test 109 between the vane span locations of 0.08 < Z / S < 0.94. The minimum radial temperature variation that was observed was approximately Δθ = 0.01 or 1% corresponding to test 126. It was decided that the results for the seven-headed thermocouple rake would be reported rather than the nine-headed since the inner most diameter thermocouple on the nine-headed rake was damaged during the first blow-down test and therefore temperature data for this rake at the inner most diameter was unavailable for all tests.

The conditions corresponding to the tests where the combustor simulator exit Re = 0.8 x 10^5, 1.1 x 10^5, 2.7 x 10^5, were given in Table 2 in italics. The measured radial temperature profiles for some of these tests are shown in Figure 12. These radial profiles have also been circum-ferentially averaged over one vane pitch. The results shown in this figure highlight that the inlet profile generator is capable of producing realistic turbine inlet profiles at any inlet Reynolds number. The measured temperature profiles show a wide range of shapes in the near ID and OD endwall regions, some having nearly uniform profiles and some having very sharp gradients. Some of the thermal profiles are peaked near the ID, some are peaked near the OD, and some are peaked near mid-span.
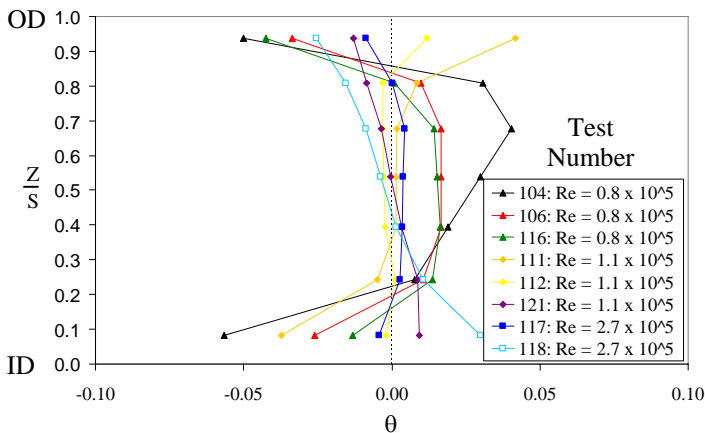

Figure 12. Several temperature profiles measured at the simulator exit at different Reynolds numbers.

The temperature profiles at the simulator exit were also found to be significantly influenced by the film cooling flow. Figure 13 shows a schematic of a generic exit temperature

profile and it illustrates some important parameters. These include the film coolant temperature, the film coolant momentum flux ratio, the near endwall temperature, and the midspan temperature. The temperature difference, $\Delta T = T_{MS} - T$, between the midspan and the near endwall flows is related to the film cooling momentum flux ratio as well as the film cooling temperature relative to the core flow near midspan. The midspan temperature is a good estimate of the core flow temperature above the film cooling holes as the flow collectively exits the simulator. The average temperature across the span at the simulator exit, T_{AVE}, is not a good choice as a scaling parameter since its value is affected by the coolant flow temperature on opposite sides of the span. The coolant exiting the film cooling holes on the ID side only sees the fluid temperature that it is being injected into locally near the ID liner, and therefore the midspan temperature is a more suitable scaling factor than the spanwise average temperature.
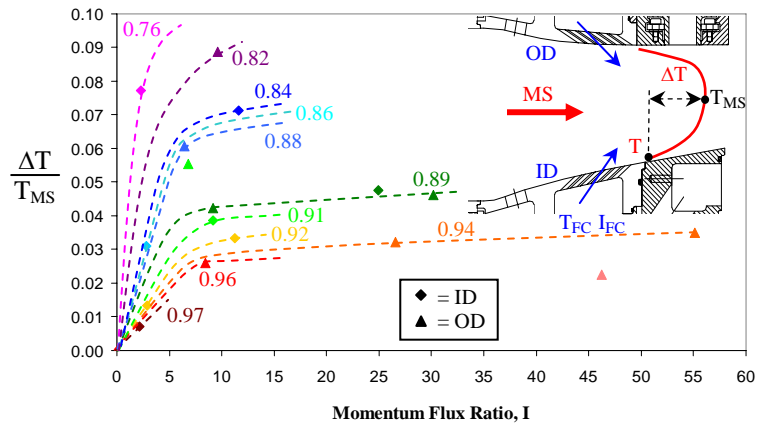

Figure 13. Plot of the near endwall temperatures as a function of film cooling temperature and momentum flux ratio for the baseline tests.

The thermal scaling for the baseline tests can also be seen in Figure 13 where ΔT has been normalized by the midspan temperature and has been plotted as a function of film cooling momentum flux ratio. Several curves are shown for different ratios of the film cooling to the midspan temperature, T_{FC}/T_{MS}. Note that the curves shown are based on the experimental data indicating the general behavior that exists for tests that resulted in a positive ΔT parameter. For a given film cooling momentum flux ratio, as the film cooling temperature is reduced relative to the midspan temperature, the larger the $\Delta T / T_{MS}$ that can be achieved. This results in increased temperature gradients near the endwall, and thus a greater potential for keeping the endwall cool. For example, when the film cooling momentum flux ratio is near I = 5, ΔT = 1% of T_{MS} when T_{FC} / T_{MS} = 97%, which corresponds to a nearly uniform exit temperature profile. However, ΔT = 9% of T_{MS} when T_{FC} / T_{MS} = 76%, which corresponds to an exit temperature profile with significant gradients near the endwalls. The figure also shows that for a given T_{FC} / T_{MS}, the relationship between ΔT and I is more sensitive for I < 10 and then gradually levels out as the momentum flux ratio is increased. These thermal trends were found for both the ID and OD film cooling.

TURBULENCE INTENSITY AND LENGTH SCALE

Turbulence intensity and length scale were investigated using TSI hotwire probes and a TSI thermal anemometry system. The

integral length scale Λ_X was determined by multiplying the mean velocity of the signal by the integral time scale T of the turbulent eddies. The integral time scale was determined by integrating the autocorrelation function R (τ) of the hotwire signal from $\tau = 0$ to a τ value corresponding to $0.00 < R (\tau) < 0.05$.

A summary of the measured turbulence intensities and length scales for three of the isothermal tests is shown in Table 3. The measured turbulence intensities were found to be in an elevated range from $20\% < Tu < 30\%$, which is consistent with real combustor exit flows as reported by Cameron et al. [7], Goebel et al. [20], and Van Fossen and Bunker [13]. The main difference between these three tests was the position (porosity) of the center shutter at the inlet of the central chamber. The position of this shutter was varied in an attempt to force different amounts of flow through the dilution holes thereby affecting the turbulence production. The integral length scales for these tests were found to scale very well with the dilution hole diameters of the simulator. The axial position of the dilution holes with respect to the location of the hotwire probes is approximately $x / D_1 = 21$ and $x / D_2 = 11$. The turbulence intensity results are consistent with some of the computational results presented in Kunze et al. [19] who performed a study that modeled the central chamber flow and thermal fields of the simulator device in this study. Note that the test numbers displayed in Table 3 correspond to the separate isothermal tests that were conducted and discussed earlier in the instrumentation section.

TABLE 3. Summary of Turbulence Intensities and Length Scales for the Isothermal Tests

Test	Tu (%)	Λ_x (m)	Λ_X / D_2
011	21.3	0.0155	0.82
013	29.8	0.0160	0.84
017	22.5	0.0190	0.99

Circumferential profiles of turbulence intensity and integral length scale near mid-span are shown in Figure 14 for one of the isothermal tests. Both profiles are plotted versus vane pitch location Y/P. The alignment of the hotwire probes with respect to the upstream dilution holes is indicated on each plot. It can be seen that as the hotwires are traversed from a circumferential position corresponding to a first row dilution hole to a circumferential position corresponding to a second row dilution hole, the turbulence intensity remains relatively constant and increases only slightly from 20% to 23%. This small increase is explained by the fact that the second row dilution holes are physically larger and closer to the hotwire probes than the first row, and therefore the turbulence associated with the second row jets is more prevalent.

Three curves are shown for both turbulence and length scale corresponding to different time averaging windows of 100 ms, 200 ms, and 300 ms. For example, the 100 ms time window means that *each* data point in that curve represents the average turbulence intensity or length scale over 100 ms and the result is plotted at the center of the time window. Three different time windows were used to determine if the calculation results would turn out consistent with one another, and from viewing Figure 14 it can be seen that this is the case. It is noted that these three time windows are much less than the overall test

time window of approximately 4.0 seconds. In the same figure, the integral length scale consistently scales well with the dilution hole diameters within the range of 80-90% of D_2 or 110-130% of D_1.
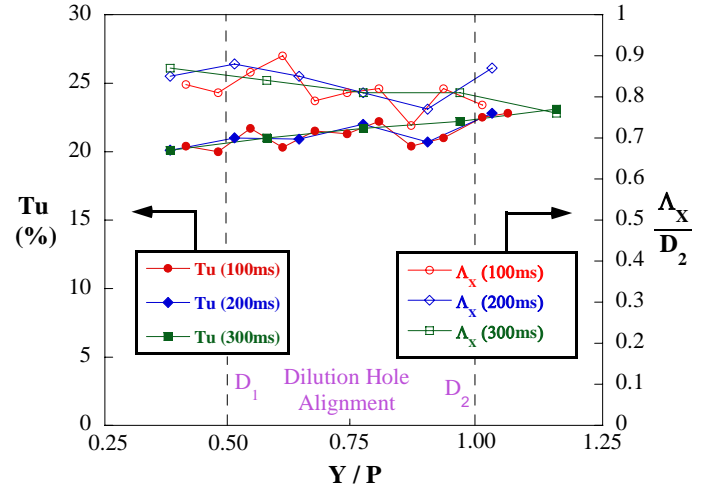

Figure 14. Plot of Tu and Λ_X at the mid-span for hotwire test 011.

CIRCUMFERENTIAL VARIATIONS

The circumferential variation in measured pressure near mid-span is shown in Figure 15 over three full vane pitches for tests 107 and 123, respectively. These two tests correspond to cases that produced spanwise pressure profiles nearly opposite of one another. Test 107 produced a spanwise pressure profile at the simulator exit that contained sharp gradients near the ID and OD endwalls with a relatively lower pressure region near mid-span, while test 123 produced a spanwise pressure profile that was peaked in the mid-span region. The total pressure has been normalized by the average pressure across the span. This normalization is more appropriate at this location than the previously defined Cp pressure coefficient which is by definition equal to zero at misdpan. This pressure ratio varies up to approximately 1.0% for test 107 and 1.5% for test 123. Relative to the spanwise pressure profile variation discussed earlier, however, no significant patterns in the pitch direction were distinguishable within the pressure waveforms. This result indicates that flow in the circumferential direction is being significantly mixed out by the highly turbulent dilution jets. This effect is not unexpected or unrealistic when compared to real combustors. The high freestream turbulence has the same effect of minimizing the circumferential variation.

The circumferential variation in measured temperature near mid-span is shown in Figure 16 over three full vane pitches for tests 107 and 127. The measured temperature has been normalized by the average temperature across the span. This temperature ratio varies up to approximately 1.0% for test 107 in which the spanwise temperature profile at the simulator exit possessed significant shape with $\Delta\theta$ near 0.1. The same temperature ratio varies by only about 0.5% for test 127 in which the spanwise temperature profile at the simulator exit is relatively uniform over the vane span. Relative to the spanwise temperature profile variation discussed earlier, no significant pitchwise patterns were distinguishable within the thermal waveforms. This result is also caused by the intense dilution mixing process which dominates the mid-span region. These effects are non uncommon in real combustors again due to the intense mixing in the circumferential direction.
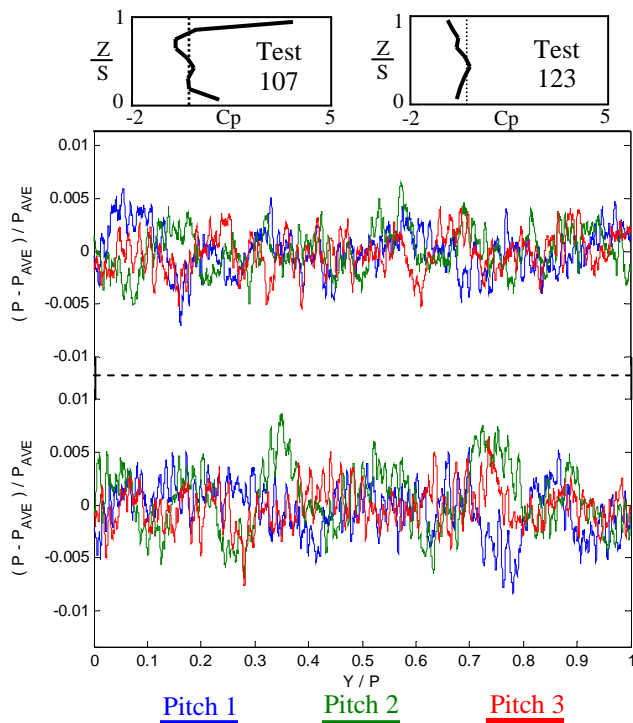
Figure 15. Circumferential pressure near mid-span over three vane pitches for tests 107 (top) and 123 (bottom).
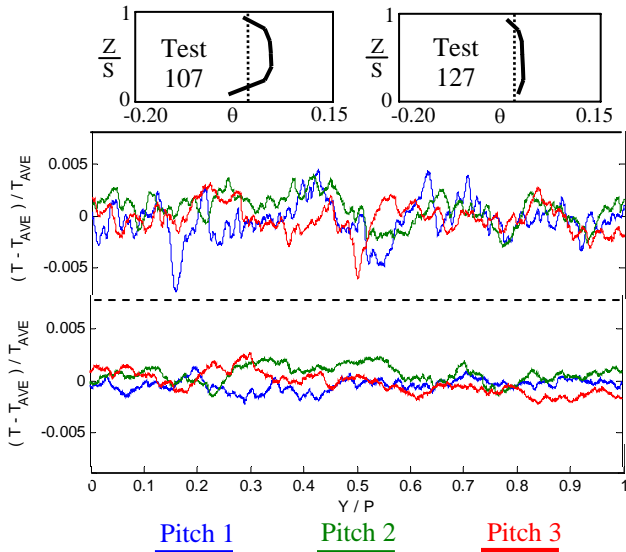

Figure 16. Circumferential temperature near mid-span over three vane pitches for tests 107 (top) and 127 (bottom).

The circumferential variation in pressure and temperature near the endwalls was observed to be similar but slightly higher than that at the midspan. The higher variation was attributed to the highly turbulent film cooling flow being located relatively closer to the exit plane than the upstream dilution holes which dominate the behavior of the profiles in the near midspan region. While the dilution holes are clocked with the vane passages, meaning that the flow for each passage is periodic, the film cooling holes are not exactly periodic for each passage due to manufacturing limitations. However, the film cooling hole periodicity, clocked with the vanes, is not relevant given that the very large number of closely spaced film cooling jets. These jets merge in the pitch direction over the twenty five cooling hole diameters of axial distance as the coolant flow approaches the vane resulting in a circumferentially uniform flow at the vane inlet along the endwalls.

It is important to note that the original design intent of this simulator device was to produce significant variations of pressure and temperature in the radial direction while also producing some variation in the circumferential direction. The results show that the central chamber configuration of the generator used in this study produced variations much more powerful in the radial direction as compared to the circumferential direction. The mean circumferential variation of pressure and temperature within most real combustors is quite low compared to that in the radial direction. In fact, as combustor designs move towards operating near stoichiometric conditions, these circumferential variations in temperature will become even less. Fuel injectors can have uneven fuel distributions, can become partially or totally clogged, misaligned, or even damaged, which can all create hot streaks and larger more significant variations in the circumferential direction, however studying these scenarios was not the goal of the current work but can be generated in future efforts.

CONCLUSIONS

The benchmark tests revealed that the inlet profile generator can produce a variety of turbine inlet profiles that are representative of actual engine conditions with realistic turbulence levels. Turbulence intensities from 20% to 30% were measured with integral length scales from 1.5 to 1.9 cm ($0.82 < \Lambda_X / D_2 < 0.99$). Pressure and temperature profiles were measured with peaks near the ID endwall, mid-span, and OD endwall. When testing at the baseline conditions, the simulator is capable of producing ID endwall pressure peaks between $-0.7 < Cp < 1.7$, OD endwall pressure peaks in the range of $-0.6 < Cp < 5.0$, and radial thermal variations up to $\Delta\theta = 10\%$ (for the seven headed thermocouple rake). Overall, the measured results show that the variation of pressure and temperature was more significant in the radial direction compared to the circumferential direction which was attributed to the high turbulence mixing out the variations.

It was shown that the exit pressure profiles in the near endwall regions scaled very well with the momentum flux ratio of the upstream film cooling flow and the combustor exit Reynolds number. The exit temperature profiles in the near endwall regions also scaled very well with the film cooling momentum flux ratio, as well as the ratio of the film cooling temperature to the midspan temperature. The liner film cooling affected the simulator exit pressure and temperature profiles between approximately $0.0 < Z / S < 0.2$ on the ID and $0.8 < Z / S < 1.0$ on the OD.

The significance of this research resides in its contribution to improving turbine engine hardware by evaluating the behavior of different combustor exit profiles. There are very few facilities that can simulate combustor profiles as inlet conditions to a full stage rotating turbine. Data sets, whether aerodynamic or heat transfer, that can be obtained from this facility will be of high value to the design community. These data sets can be used to baseline CFD codes allowing more confident extrapolation of the codes to the specific profiles and turbine that the designer wishes.

The results from the current study are useful to engine designers of both aircraft and power generation turbines since they show how a single combustor geometry can produce widely different flow and thermal field conditions entering the downstream turbine. The results show that great emphasis should be placed on obtaining accurate knowledge of the flow distribution within the combustion chamber at all operating conditions. This distribution is paramount and the results show that analyzing the performance of turbine hardware should be conducted using more precise profiles rather than uniform inlet conditions typically used in the past. Turbine inlet profiles possessing significantly different shapes can alter the flow physics in the turbine vane and blade passages thereby changing local aerodynamics and heat transfer.

This study will be used as a launching point for future studies. These include analyses of the surface heat transfer and loading changes as a result of the variation in inlet profile. Another future study involves understanding the loss mechanisms as a result of different secondary flow development within the turbine. Endwall heat transfer will also be investigated with this profile generator Other studies will involve modifying dilution hole patterns to increase circumferential variations of pressure and temperature with the specific goal of studying combustor hot streaks and migration patterns.

ACKNOWLEDGMENTS

REFERENCES

[1] Barringer, M., Thole, K., and Polanka, M., 2004, "Developing a Combustor Simulator for Investigating High Pressure Turbine Aerodynamics and Heat Transfer," ASME GT2004-53613.

[2] Barringer, M., Thole, K., and Polanka, M., 2006, "Effects of Combustor Exit Profiles on High Pressure Turbine Vane Aerodynamics and Heat Transfer," ASME GT2006-90277.

[3] Holdeman, J.D., 1993, "Mixing of Multiple Jets with a Confined Subsonic Crossflow," *Prog. Energy Combustion. Science.*, Vol. 19, pp. 31-70.

[4] Ames, F.E. and Moffat, R.J., 1990, "Effects of Simulated Combustor Turbulence on Boundary Layer Heat Transfer," Heat Transfer in Turbulent Flow 1990: AIAA/ASME Thermophysics and Heat Transfer Conference, Seattle, Wash., June 18-20, 1990.

[5] Barringer, M., Richard, O., Stitzel, S., Walter, J., and Thole, K., 2002, "Flow Field Simulations of a Gas Turbine Combustor," *J. of Turbomachinery*, Vol. 124, pp. 508-516.

[6] Stitzel, S. and Thole, K. A., 2003, "Flow Field Computations of Combustor-Turbine Interactions Relevant to a Gas Turbine Engine," ASME GT-2003-38253.

[7] Cameron, C., Brouwer, J., Wood, C., and Samuelsen, G., 1989, "A Detailed Characterization of the Velocity and Thermal Fields in a Model Can Combustor with Wall Jet Injection," *J. of Eng. for Gas Turbines and Power*, Vol. 111, pp. 31-35.

[8] Bicen, A., Tse, D., and Whitelaw, J., 1988, "Flow and Combustion Characteristics of an Annular Combustor," *Combustion and Flame*, Vol. 72, pp. 175-192.

[9] Schwab, J., Stabe, R. and Whitney, W., 1983, "Analytical and Experimental Study of Flow Through an Axial Turbine Stage With a Nonuniform Inlet Radial Temperature Profile," AIAA 83-1175.

[10] Cattafesta, L., 1988, "An Experimental Investigation of the Effects of Inlet Radial Temperature Profiles on the Aerodynamic Performance of a Transonic Turbine Stage," Masters Thesis, M.I.T.

[11] Chana, K., Hurrion, J., Jones, T., 2003, "The Design, Development and Testing of a Non-Uniform Inlet Temperature Generator for the QinetiQ Transient Turbine Research Facility," ASME 2003-GT-38469.

[12] Krishnamoorthy, V., Pai, B., and Sukhatme, S., 1988, "Influence of Upstream Flow Conditions on the Heat Transfer to Nozzle Guide Vanes," *J. of Turbomachinery*, Vol. 110, pp. 412-416.

[13] Van Fossen, J. and Bunker, R., 2002, "Augmentation of Stagnation Region Heat Transfer Due to Turbulence from an Advanced Dual-Annular Combustor," ASME GT2002-30184.

[14] Colban, W., Thole, K., and Zess, G., 2002, "Combustor Turbine Interface Studies – Part 1: Endwall Effectiveness Measurements," ASME 2002-GT-30526.

[15] Hermanson, K. and Thole, K., 2000, "Effect of Inlet Conditions on Endwall Secondary Flows," AIAA 99-0241.

[16] Haldeman, C. W., Dunn, M. G., MacArthur, C. D., and Murawski, C. G., 1992, "The USAF Advanced Turbine Aerothermal Research Rig (ATARR)," NATO AGARD Propulsion and Energetics Panel Conference Proceedings 527, Antalya, Turkey.

[17] Roy, Ranjit K., Design of Experiments Using the Taguchi Approach., John Wiley & Sons, Inc., New York, 2001.

[18] Kunze, V., Wolff, M., Barringer, M., Thole, K., and Polanka, M., 2006, "Numerical Insight Into Flow and Thermal Patterns Within an Inlet Profile Generator Comparing to Experimental Results," ASME GT2006-90276.

[19] Kunze, V., Wolff, M., Barringer, M., Thole, K., and Polanka, M., 2005, "Numerical Modeling of Flow and Thermal Patterns Within a Combustor Simulator," ASME GT2005-68284.

[20] Goebel, S., Abuaf, N., and Lee, C., 1993, "Measurements of Combustor Velocity and Turbulence Profiles," ASME Paper No. 93-GT-228.